Proton-Dependent Electron Transfer from Cu_A to Heme *a* and Altered EPR Spectra in Mutants Close to Heme *a* of Cytochrome Oxidase[†]

Denise A. Mills,[‡] Shujuan Xu,[§] Lois Geren,[||] Carrie Hiser,[‡] Ling Qin,[‡] Martyn A. Sharpe,[‡] John McCracken,[§] Bill Durham,[||] Francis Millett,*[,||] and Shelagh Ferguson-Miller*[,‡]

Departments of Biochemistry and Molecular Biology and Chemistry, Michigan State University, East Lansing, Michigan 48824, and Department of Chemistry and Biochemistry, University of Arkansas, Fayetteville, Arkansas 72701

Received June 19, 2008; Revised Manuscript Received September 5, 2008

ABSTRACT: Eukaryotic cytochrome *c* oxidase (C*c*O) and homologous prokaryotic forms of *Rhodobacter* and *Paraccocus* differ in the EPR spectrum of heme *a*. It was noted that a histidine ligand of heme *a* (H102) is hydrogen bonded to serine in *Rhodobacter* (S44) and *Paraccocus* C*c*Os, in contrast to glycine in the bovine enzyme. Mutation of S44 to glycine shifts the heme *a* EPR signal from $g_z = 2.82$ to 2.86, closer to bovine heme *a* at 3.03, without modifying other properties. Mutation to aspartate, however, results in an oppositely shifted and split heme *a* EPR signal of $g_z = 2.72/2.78$, accompanied by lower activity and drastically inhibited intrinsic electron transfer from Cu_A to heme *a*. This intrinsic rate is biphasic; the proportion that is slow is pH dependent, as is the relative intensity of the two EPR signal components. At pH 8, the heme *a* EPR signal at 2.72 is most intense, and the electron transfer rate (Cu_A to heme *a*) is $10-130\ s^{-1}$, compared to wild-type at $90000\ s^{-1}$. At pH 5.5, the signal at 2.78 is intensified, and a biphasic rate is observed, 50% fast (∼wild type) and 50% slow ($90\ s^{-1}$). The data support the prediction that the hydrogen-bonding partner of the histidine ligand of heme *a* is one determinant of the EPR spectral difference between bovine and bacterial C*c*O. We further demonstrate that the heme *a* redox potential can be dramatically altered by a nearby carboxyl, whose protonation leads to a proton-coupled electron transfer process.

Cytochrome *c* oxidase (C*c*O)[1] is the terminal electron acceptor in the respiratory chain of mammalian mitochondria. It contains multiple redox-active metal centers through which electrons are transferred from the soluble electron donor cytochrome *c* (C*c*) to oxygen. The initial electron acceptor in C*c*O is a dinuclear Cu_A in subunit II (Figure 1). The electron is transferred next to heme *a*, a low-spin six-coordinated heme with two axial histidine ligands (H102 and H421) and then to Cu_B and heme a_3 (with one axial ligand, H419); the latter pair make up the active site where oxygen is reduced to water. The movement of electrons through C*c*O is energetically downhill and is coupled to the movement of protons across the membrane, creating an electrochemical potential across the respiratory membrane that drives the synthesis of ATP (*1*). The mechanism of coupling between proton transfer and electron transfer is not fully understood.

Although heme *a* is not directly involved in the catalysis of O_2 reduction to H_2O, it is proposed that heme *a* reduction is linked to redox changes at the binuclear site (*2*−*4*), exhibiting negative cooperativity with the closely located heme a_3 (*5*), and is probably linked to the movement of protons as well (*6, 7*). There is a high degree of conservation of sequence and structure between the prokaryotic and eukaryotic C*c*Os in their three core subunits and metal sites (*8*−*10*), leading to bacterial C*c*Os being good model systems for the more complex mammalian enzymes. However, there are differences, including a higher steady-state activity for the *Rhodobacter sphaeroides* (*Rs)* and *Paracoccus denitrificans* (*Pd*) bacterial C*c*Os than the bovine C*c*O and a 1−2 nm red shift in the visible spectrum, Soret and α peaks (*11*). In addition, the redox potential of bovine heme *a* is measured to be more positive, by ∼+13 mV, relative to the *Rs* heme *a* (*12, 32*), assuming similar redox potentials of Cu_A. Interactions of an arginine with the formyl group of heme *a* have been shown to have an important influence on the redox potential (*13*). But this interaction is observed to be similar in bovine, *Pd*, and *Rs* C*c*O, with a specific vibrational mode in resonance Raman at $1610\ cm^{-1}$ (*14, 15*).

The g_x, g_y, g_z values of the EPR spectrum of heme *a* in the bacterial oxidases (*Pd* and *Rs*) are shifted relative to bovine oxidase; in particular, the g_z band is 2.82 in *Rs* compared to 3.03 in bovine (*11*). It was speculated, even

[†] Supported by National Institutes of Health Grants GM26916 (S.F.-M.), GM54065 (J.M.), and GM20488 (F.M. and B.D.) and NCRR COBRE P20 RR15569 (F.M. and B.D.).

* To whom correspondence should be addressed. S.F.-M: telephone, (517) 353-0199; fax, (517) 353-9334; e-mail, fergus20@msu.edu. F.M.: telephone, (479) 575-4999; fax, (479) 575-4049; e-mail, millett@uark.edu.

[‡] Department of Biochemistry and Molecular Biology, Michigan State University.

[§] Department of Chemistry, Michigan State University.

[||] Department of Chemistry and Biochemistry, University of Arkansas.

[1] Abbreviations: C*c*O, cytochrome *c* oxidase; C*c*, cytochrome *c*; COV, cytochrome *c* oxidase in phospholipid vesicle (proteoliposome); 3CP, 3-carboxy-2,2,5,5-tetramethyl-1-pyrrolidinyloxy free radical; DEAE, diethylaminoethyl; EPR, electron paramagnetic resonance; LM, lauryl maltoside; *Pd*, *Paracoccus denitrificans*; PCR, polymerase chain reaction; *Rs*, *Rhodobacter sphaeroides*; RCR, respiratory control ratio; RuC*c*, ruthenium complex-labeled cytochrome *c*; Ru_2Z, ruthenium dimer; TMPD, *N*,*N*,*N*′,*N*′-tetramethyl-*p*-phenylenediamine.

10.1021/bi801156s CCC: $40.75
Published on Web 10/11/2008

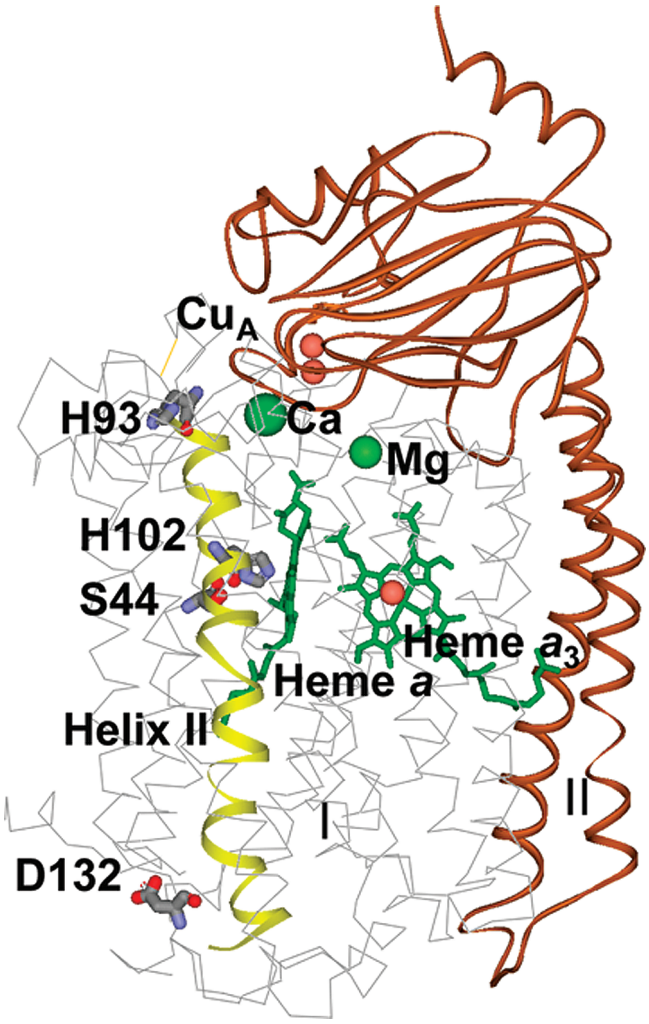

FIGURE 1: The structure of the two subunits of *Rs* C*c*O from 2GSM (*10*) is shown with subunit I (gray) containing heme *a* and a_3 (green sticks) and Cu_B as an orange sphere, with the metals of Ca and Mg (green spheres) close to the subunit I/II interface. Key residues are shown (sticks) on helix I (yellow ribbon): H93, H102 (a ligand of heme *a*), S44, and D132 at the entrance of the proton uptake path. Subunit II (red) is shown with its dinuclear Cu_A (orange spheres).

before the advent of a crystal structure, that the shifted EPR *g* values in *Rs* C*c*O could be explained by an increased anionic character of one or both of the heme *a* histidine axial ligands, possibly due to altered hydrogen bonding of the histidines to nearby residues (*11*). Examination of the crystal structures of bovine C*c*O (*16*) revealed that the peptide backbone oxygen of a conserved glycine in subunit I is hydrogen bonded to a histidine ligand of heme *a* in all mammalian aa_3-type oxidases and in many other species including yeast, wheat, and *Thermus thermophilus* ba_3 oxidase (*17*). However, in the bacterial aa_3 oxidases from *Pd* and *Rs*, the glycine has been replaced with a serine (Figure 2) with the hydroxyl group of the serine (S44) hydrogen-bonded to H102. The other histidine ligand of heme *a* (H421) is surrounded by highly conserved hydrophobic/aromatic amino acids which coincide in an overlay of the *Rs* and bovine structures and thus are not a likely source of altered heme *a* properties.

To test the possible effect of hydrogen bonding to the histidine ligand of heme *a*, the serine 44 residue in *Rs* C*c*O was mutated to a glycine, creating a bovine-like mutant form,

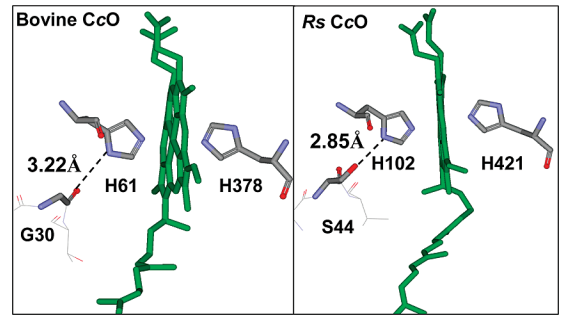

FIGURE 2: The ligands to heme *a* are shown for bovine (2DYR, oxidized structure) and *Rs* (2GSM, oxidized structure) C*c*O. The residues that are closest to the heme *a* ligands are shown in sticks. Bovine C*c*O shows a glycine (G30) with the carbonyl backbone oxygen hydrogen-bonding to His 61. *Rs* C*c*O shows a serine (S44) with its hydroxyl hydrogen-bonding to His 102.

S44G. The S44 was also replaced by an aspartic acid group, S44D, to observe the effect of a negatively charged residue on the histidine ligand, with the expectation that the S44G would shift the EPR spectrum closer to bovine, while the S44D might move it further away. This expectation was met, and further, the S44D mutant (but not a control mutant, S44N) significantly altered the electron transfer and redox properties of heme *a*, leading to unique insights into the control of heme *a* redox behavior and a new tool for studying the coupling of electron and proton movement.

METHODS

Site-Directed Mutagenesis and Protein Purification. The Macromolecular Structure, Sequencing, and Synthesis Facility of the MSU Research Technology Support Facility synthesized all PCR primers and sequenced all mutated genes entirely. To create the S44G mutant, the central 1037 bp *Nco*I fragment of the *cox*I gene was mutated by the splicing-by-overlap-extension PCR method (*18*). The internal primers 5′-GTCGATC**GG**GGTGGCCTTCAC-3′ and 5′-CCAC-C**CC**GATCAGCCCGACGAG-3′ were used in conjunction with the external M13 forward and M13 reverse primers. The mutated S44G *cox*I *Nco*I piece was then ligated back into the rest of the 6-histidine-tagged *cox*I gene from pJS3-SH (*19*). To create the S44D mutant, the full-length 6-histidine-tagged *cox*I gene was mutated by the QuikChange mutagenesis procedure (Stratagene). Primers were 5′-CTGATC**GAC**GTGGCCTTCACCGTCTACA-3′ and 5′-**GTC**GATCAGCCCGACGAGGCCCCCGGTGA-3′. Subsequently, a *Hin*dIII site was inserted into the *Eco*RI site upstream of the *cox*I gene in each mutated plasmid. The complete mutant *cox*I genes could then be isolated with *Hin*dIII and ligated into *Hin*dIII-cut pRK415 (*20*). The resulting plasmids were cut with *Pst*I and ligated with the operon containing the wild-type *cox*II and *cox*III genes (*21*) to create the final expression plasmids pCH252 (S44G) and pCH331 (S44D). These plasmids were first transformed into *Escherichia coli* S17-1 (*22*) and then transferred by conjugation from S17-1 to *R. sphaeroides* strains JS100 (*23*) or Δ123 (*10*), respectively, as described (*24*).

To create the S44N and S44E mutants, the same fragment of *cox*I was mutated by the QuikChange mutagenesis procedure (Stratagene). Primers were 5′-CGGGCTGAT-C**AAC**GTGGCCTTCA-3′ and 5′-GCCAC**GTT**GATCAGC-CCGACGAG-3′ for S44N. The mutated *cox*I *Nco*I piece was

Table 1: Activities of Reconstituted Wild-Type and S44D C*c*O Measured by Stopped Flow as a Function of pH and in the Presence or Absence of Zinc

		activity ($e^- s^{-1} aa_3^{-1}$)		
pH	COVs	controlled	uncontrolled	RCR
6.5	WT	130 ± 12	950 ± 24	7.3
7.4		80 ± 1	1050 ± 28	13
7.4 + Zn		16 ± 1	573 ± 3	36
6.5	S44D	90 ± 1	297 ± 15	3.3
7.4		47 ± 1	185 ± 5	3.9
7.4 + Zn		8 ± 1	97 ± 9	12

then ligated back into the rest of the 6-histidine-tagged *cox*I gene from pJS3-SH (*19*). Cytochrome *c* oxidase was extracted from *Rs* grown in Sistrom's media as described (*11*) and purified on a Ni-NTA affinity column (*24*). Solubilized membrane proteins were suspended in buffer (10 mM Tris-HCl, pH 8.0, 10 mM imidazole, 40 mM KCl, and 0.1% lauryl maltoside (LM) and then poured over a Ni-NTA column (Qiagen), followed by washing without imidazole and elution with 80 mM histidine in 10 mM Tris-HCl, pH 8.0, 40 mM KCl, and 0.1% LM. The protein, after Ni-NTA affinity chromatography, was further washed with 20 mM HEPES−KOH, pH 7.4, 0.1% LM, and 15 mM KCl using a Amicon Ultra 100 concentrator to remove Ni-histidine. Further ion-exchange chromatography was used with two DEAE columns in tandem (Tosohaas DEAE-5PW 10 μm particle size, 8 mm × 7.5 cm) using a Pharmacia ÃKTA FPLC as previously described (*24*).

Visible Spectral Analysis of S44 Mutants. Spectrophotometric analysis of the hemes in *Rs* C*c*O was performed using a Perkin-Elmer Lambda 40P to scan the wavelengths from 250 to 700 nm under resting, oxidized, reduced with sodium dithionite, and reduced with CO-bound conditions, as described in the figure legends.

EPR Measurements. X-band EPR spectra of the purified *Rs* C*c*O WT and S44G, S44D, and S44N mutants were measured with a Bruker ESP-300E spectrometer equipped with a TE_{102} cavity. Temperature was maintained at 4.2 K using an Oxford helium cryostat assembly. The *g* values were determined by direct measurements of the magnetic field strength and microwave frequency. Spectrometer conditions: microwave frequency, 9.458 GHz; microwave power, 50 μW; modulation amplitude, 20.0 G.

Activity of COVs under Steady-State and Stopped-Flow Proton Pumping Measurements. C*c*O was reconstituted into asolectin lipid vesicles (COVs) using a dialysis method as previously described (*25*). Measurements of proton pumping were made on an OLIS-rsm stopped flow with 100 μM phenol red, 50 μM HEPES−KOH, pH 7.4, plus 45 mM KCl on the outside of the COVs and 75 mM HEPES−KOH, pH 7.4, on the inside. Activities were obtained from averaging at least three measurements of cytochrome *c* oxidation from scanning a range of 155 nm (472−627 nm) using double monochromators with a 500 blaze wavelength and a groove density of 600 lines. The rapid scanning of the wavelength range was at the rate of 1 scan/ms. The OLIS-rsm SVD Global Works software package was used to analyze the spectra. Additionally, exponential fitting of the cytochrome *c* changes monitored at 550 nm using Microcal Origin, in the absence of phenol red, was performed. The activities of the COVs were measured in the absence of ionophores, forming both a membrane potential and a pH gradient during turnover (controlled state). The addition of valinomycin to COVs removes the $\Delta\Psi$, and this is the condition in which proton pumping is normally observed as a net acidification (decrease in absorbance) of the phenol red on the outside. The addition of FCCP removes the pH gradient (uncontrolled state) by allowing protons to equilibrate across the membrane, resulting in alkalinization on the outside (increase in absorbance), due to the net consumption of protons for the formation of H_2O at the active site.

Scheme 1

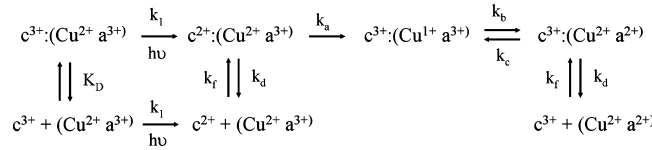

Steady-state activities were measured in a Gilson oxygraph with a Clark-type electrode. Ascorbate and TMPD were added to reduce horse heart cytochrome *c*, the electron donor to C*c*O, under conditions described in the legend to Table 1.

Photoinduced Electron Transfer Measurements. Ruthenium-labeled cytochrome *c* derivatives were used to deliver electrons to the oxidized C*c*O using laser flash photolysis (*26*). Horse Ru-39-C*c* was prepared by labeling the horse K39C mutant with (4-bromomethyl-4′-methylbipyridine)(bis-bipyridine)ruthenium(II) as described (*26*). The horse K39C C*c* mutant was prepared using the method of Patel et al. (*27*) and will be described elsewhere (*28*). Horse Ru-72-C*c* was prepared as described by Liu et al. (*29*). The ruthenium dimer Ru_2Z was synthesized as described by Brand et al. (*30*). Laser flash photolysis was carried out as described by Geren et al. (*26*), in which the photoexcited state Ru(II*) rapidly transferred an electron to heme *c*. The excitation pulse was provided by a phase R Model DL1400 flash lamp-pumped dye laser using coumarin 490 to produce a 480 nm light flash of <0.5 μs duration. At low ionic strength, Ru-39-C*c* forms a 1:1 complex with C*c*O so that rapid electron transfer from heme *c* to Cu_A and heme *a* in C*c*O can be measured spectrophotometrically at 550, 830, and 605 nm, respectively. The reaction of cytochrome *c* was monitored at 550 nm using an extinction coefficient of $\Delta\varepsilon_{550} = 18.5$ mM^{-1} cm^{-1}. The reaction of Cu_A was monitored at 830 nm using $\Delta\varepsilon_{830} = 2.0$ mM^{-1} cm^{-1}, and the reduction of heme *a* was measured at 605 nm using $\Delta\varepsilon_{605} = 16$ mM^{-1} cm^{-1}. In some experiments, heme *a* was monitored at 600 nm using an interference filter with 10 nm bandwidth and an effective extinction coefficient of 9.6 mM^{-1} cm^{-1} (*31*). Reaction solutions typically contained 5−15 μM Ru-C*c*, 5−20 μM C*c*O, 10 mM aniline, and 1 mM 3CP in 5 mM Tris-HCl, pH 8.0, at 22 °C. The aniline and 3CP function as sacrificial electron donors to reduce Ru(III) and prevent the back-reaction. Ionic strength was increased with addition of up to 300 mM NaCl. The transients were fitted to appropriate theoretical equations for Scheme 1 as described by Geren et al. (*26*). Each measurement was repeated at least three times, and the errors reported are standard deviations.

RESULTS

Optical Spectra and Activity. The mutation S44G in *Rs* C*c*O does not cause any alteration of the visible spectrum

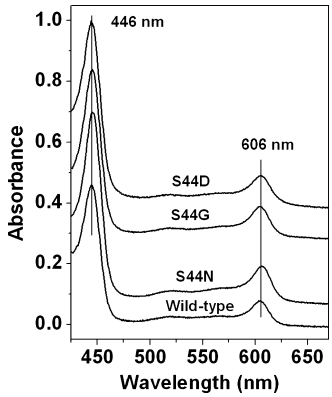

FIGURE 3: The UV−vis spectra of reduced wild-type and S44D, S44G, and S44N *Rs* C*c*O. All show normal Soret (446 nm) and α (606 nm) band peaks. Buffer contained 200 mM HEPES−KOH, pH 7.4, and 0.1% dodecyl maltoside with sodium dithionite as a reductant.

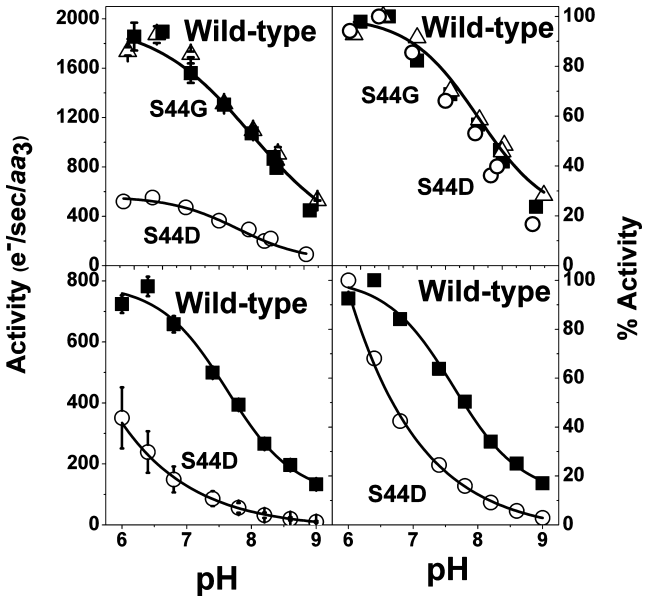

FIGURE 4: The top two panels show the steady-state activity of S44G (△), S44D (○), and wild-type (■) *Rs* C*c*O at different pH values over the pH range 6−9, with errors bars shown if significant. The lower two panels show the stopped-flow rates of activity, in which the cytochrome *c* is not saturating. The left panels show the activity (e^- s^{-1} aa_3^{-1}), and the right panels show the percentage activity. The buffers MES−KOH, HEPES−KOH, and CHES−KOH were used at 50 mM with appropriate amounts of KCl to give approximate ionic strength of 45 mM with respect to potassium and with dodecyl maltoside at 0.1%.

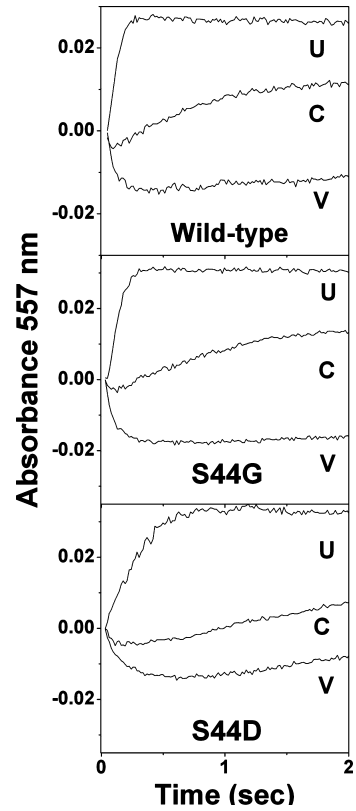

FIGURE 5: Measurements of proton uptake and release by wild-type, S44G, and S44D C*c*O in proteoliposomes (COVs) using the externally added pH-sensitive dye, phenol red. The assays contained 0.1 μM aa_3 with pH adjusted to pH 7.4 with 50 μM HEPES−KOH on the outside and 75 mM HEPES−KOH on the inside. Increasing absorbance in the controlled state, C, indicates alkalinization on the outside of COVs as a result of proton backflow due to a high $\Delta\Psi + \Delta pH$. Addition of valinomycin, V, relieves the $\Delta\Psi$, resulting in a decrease in absorbance consistent with proton pumping to the outside of the COVs. In the uncoupled state, U, addition of FCCP results in net alkalinization, as protons are consumed in the reduction of oxygen to water and equilibrate across the membrane.

compared to wild type (Soret peak at 445nm; α peak at 606 nm), suggesting that there are no major changes in the overall protein structure (Figure 3). Additionally, the maximal activity across the pH range from pH 6 to pH 9 is not altered (Figure 4). Thus, the mutation to a glycine does not change any rate-limiting step in the steady-state turnover. When reconstituted into COVs, S44G gives good proton pumping with an H^+/e^- ratio similar to wild type (Figure 5). The mutation S44N also causes no alteration in the visible spectrum (Figure 3) or in the overall activity (see below).

The S44D mutation was also spectrally similar to wild-type *Rs* C*c*O (Figure 3), although heme *a* showed a slightly lowered apparent extinction (∼10−20%) based on the ratio of the reduced α band to the reduced Soret. The reduced CO-bound form was similar to wild type, indicative of a normal low-spin heme *a* (data not shown). However, activity at pH 6.5, under maximal steady-state conditions, of the S44D mutant (500 ± 50 s^{-1}) was only 30% of the wild-type activity (1700 ± 300 s^{-1}), while that of S44G and S44N (1500 ± 90 s^{-1}) was very similar to wild type. When reconstituted into COVs, S44D showed a lowered respiratory control ratio (RCR = uncontrolled rate/controlled rate). The decreased RCR of S44D is observed in both steady-state (data not shown) and pre-steady-state stopped-flow measurements of COVs (Table 1), indicating differentially slower uncontrolled rate at pH 6.5 and 7.4. Proton pumping was consistently found to be somewhat less in S44D (<0.5 H^+/e^-) than wild type or S44G (Figure 5). However, both wild type and S44D are equally inhibited by zinc, 80% and 82%, respectively, added to the outside of COVs (Table 1). This measurement was made to test whether protons from a backflow pathway from the external bulk solution (apparently blocked by Zn^{2+} (*25*)) might be supporting the protonation of S44D; the results suggest not (see p 24).

The effect of pH on the steady-state activity of the S44D mutant, using saturating levels of cytochrome *c*, was the same as for wild type with an apparent pK_a of 7.6, although with much lower activity (Figure 4, top panel). However, in stopped-flow analysis, under conditions used for proton

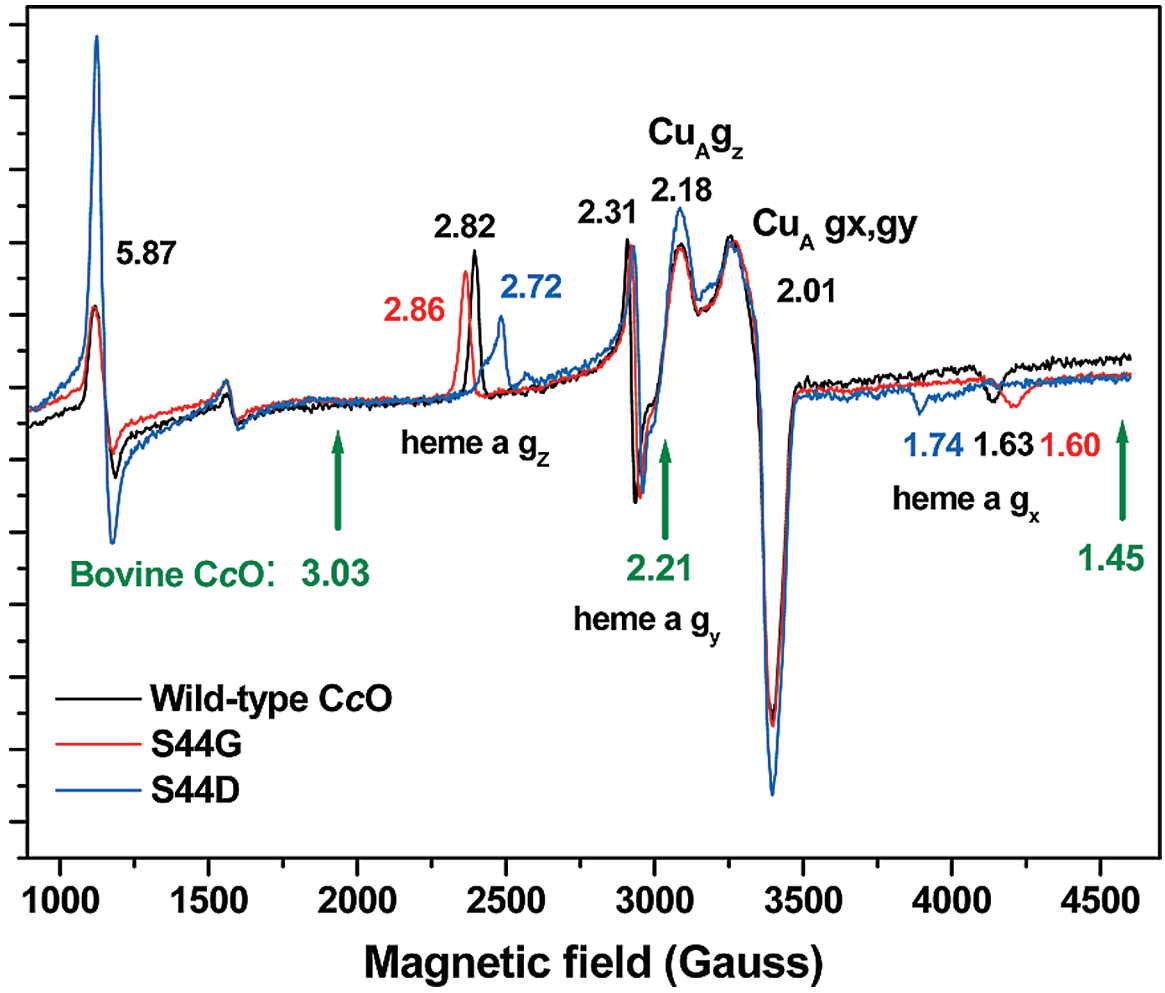

FIGURE 6: EPR spectra of wild-type *Rs* C*c*O (black line), and mutants, S44G (red line) and S44D (blue line), with bovine *g* values (green) below the spectra and indicated with green arrows. The g_z, g_x, g_y values are given for the g_z, g_x, and g_y of heme *a*. (See also Table 2.) Samples were made in a buffer of 20 mM HEPES−KOH, pH 8.0, 14 mM KCl, and 0.1% lauryl maltoside with final concentrations of 82, 88, and 61 μM C*c*O, respectively. EPR experimental conditions: microwave frequency, 9.458 GHz; microwave power, 50 μW; modulation frequency, 100 kHz; modulation amplitude, 20.0 G; conversion time, 327 ms; temperature, 4.2 K.

pumping measurements where C*c* levels are nonsaturating and electron input is rate-limiting, there was a considerably different pH profile for S44D with an apparent pK_a < 6 (Figure 4, lower panel), compared to a pK_a of 7.2 for wild-type C*c*O. This finding is consistent with observations of a severely inhibited Cu_A to heme *a* intrinsic electron transfer rate (see below), which presumably becomes more dominant in the overall rate when Cu_A is not kept fully reduced. The fact that the overall rate at low pH is ~500 s^{-1} while the intrinsic rate can be as low as 10−100 s^{-1} undoubtedly reflects the very different conditions of ionic strength and C*c* concentration used in the different measurements, as well as the enzyme's response to multiple turnover versus single electron input conditions.

EPR Spectroscopy. The EPR spectrum of wild-type *Rs* C*c*O shows heme *a* *g* values of $g_z = 2.82$, $g_x = 2.31$, and $g_y = 1.63$ (Figure 6), the same as wild-type *Pd* C*c*O (*11*), whereas the bovine oxidase has distinctly different *g* values for heme *a* of $g_z = 3.03$, $g_x = 2.21$, and $g_y = 1.45$ (Figure 6, arrows). In contrast, the EPR spectral features of Cu_A in wild-type *Rs* C*c*O differ little from the bovine ($g_z = 2.18$ and g_x, $g_y = 2.01$). The mutant forms of *Rs* C*c*O at position 44, created to test its role in determining the heme *a* differences, were, as expected, essentially unaltered in this dinuclear Cu_A center.

Table 2: Summary of the Heme *a* EPR g_x, g_y, and g_z Values of the Wild-Type and S44 Mutants of *Rs* C*c*O

C*c*O	g_z	g_y	g_x
Rs wild type	2.82	2.31	1.63
S44D	2.72/2.78	2.31	1.74
S44G	2.86	2.30	1.60
S44N	2.80	2.31	1.65
bovine C*c*O	3.03	2.21	1.45

The mutation of S44 in *Rs* C*c*O to glycine, to match bovine C*c*O, did produce an altered EPR spectrum of heme *a* with $g_{z,x,y}$ values of 2.86, 2.30, and 1.60 (Figure 6). These values are closer to those of bovine C*c*O in all cases, though not shifted as dramatically as would be expected if this residue were the sole contributor to the difference between *Rs* and bovine C*c*O.

The S44D mutation, while minimally perturbing the visible spectra, shows markedly different $g_{x,y,z}$ values from wild- type and S44G, with two peaks for $g_z = 2.72/2.78$ and two peaks for $g_y = 1.74/1.68$, which are considerably shifted in the direction opposite to those of bovine and of the S44G mutant (Figure 7A). When the EPR spectra were measured at different pH values from pH 5.5 to pH 8.0, there was a marked shift in the relative intensities of the two peaks: g_z 2.72 was strongest at high pH and g_z 2.78 had increased

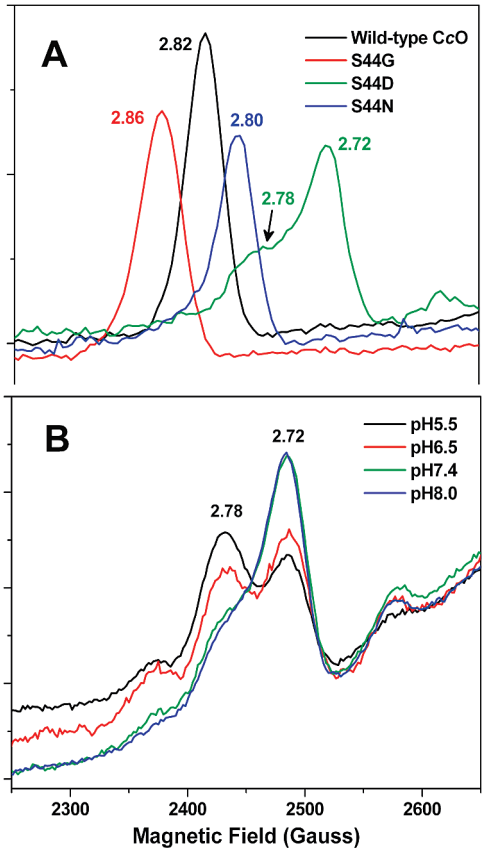

FIGURE 7: (A) Overlay of the EPR spectral changes with wild-type *Rs* C*c*O (black), S44G (red), S44D (green), and S44N (blue) in 20 mM HEPES−KOH, pH 8.0, 14 mM KCl, and 0.1% lauryl maltoside. The EPR spectra were measured with a microwave frequency of 9.458 GHz, a microwave power of 50 μW, and a modulation amplitude of 20.0 G at 4.2 K. (B) Effect of pH on the amplitude of the heme *a* g_z EPR spectra of S44D. 50 mM MES−KOH buffer was used for pH 5.5 and 6.5 with 0.1% lauryl maltoside, whereas pH 7.4 and 8.0 buffers contained 50 mM HEPES−KOH and 0.1% lauryl maltoside. Ionic strength was controlled by adjusting the conductivity with NaCl. Colored lines are shown for pH 5.5 (black), pH 6.5 (red), pH 7.4 (green), and pH 8.0 (blue). EPR conditions are described in Methods. The changes in the split 2.72/2.78 peaks, with pH change, are depicted.

intensity at low pH, indicating that the EPR signal is influenced by a protonation event (Figure 7B). Spin quantification by double integration of these two peaks shows that the total area under the peaks is comparable in magnitude at different pH values, indicating an interconversion between them. The results are consistent with the 2.78 peak representing the protonated form of Asp44 and 2.72 the unprotonated. When the areas under the two peaks are plotted as a function of pH, the p*K* of the interconversion appears to be <5.5, the lowest pH that can be measured. This value is also consistent with the results of kinetic measurements of the proportion of fast and slow intrinsic electron transfer rates from Cu_A to heme *a* (see below and Figure 13).

EPR spectra of samples at different ionic strength were also studied. Higher ionic strength had the same effect on S44D as lowering pH, making the peak at 2.78 more intense, although not as dramatic an effect as pH. Similarly, cytochrome *c* binding caused a small shift in the relative intensities of the 2.78/2.72, in this case lowering the intensity of the 2.78 peak, as in high pH (data not shown).

As a control for the effect of charge/protonation state in the S44D mutation, asparagine was also substituted at position 44 and produced a similar direction of EPR shift as S44D but had a single peak at $g_z = 2.80$, close to that of the apparent protonated form of S44D, and was wild type in overall activity.

In the EPR spectrum of the S44D mutant of *Rs* C*c*O, a large signal appears at $g_z = 5.87$. This "$g_z = 6$" signal is normally attributed to high-spin heme a_3. In wild-type C*c*O, due to antiferromagnetic coupling between high-spin heme a_3 and Cu_B, little or no EPR signal is seen in this region. In some cases, if the binuclear center is not perfectly coupled, a weak signal from heme a_3 appears in this region in bovine C*c*O. The presence of the signal in the S44D mutant suggests a decoupling that could be the result of some reduction of Cu_B due to the very low redox potential of heme *a* (see Discussion).

An interesting feature of *Rs* C*c*O is that the magnesium site that is centrally located at the interface of subunits I and II (Figure 1) can be substituted with Mn, creating a fully active form of the enzyme with a strong EPR signal that is sensitive to any conformational changes in the region (*11*). Studies showed that the Mn spectrum is not altered by any of the S44 mutations. In S44D, the spectrum of Mn is also unaffected by buffer pH, indicating no general conformational change is involved in the EPR spectral changes observed in heme *a*.

Photoinduced Electron Transfer Measurements. Rapid electron transfer was studied using Ru-39-C*c*, which contains a ruthenium complex covalently attached to Cys-39 on the back surface of C*c* remote from the binding domain. The ruthenium complex at this position does not affect the binding of C*c* to C*c*O or the second-order rate constant of the reaction between the two proteins (*26*). Photoexcitation of the ruthenium complex on Ru-39-C*c* leads to rapid electron transfer from the excited-state Ru(II*) to heme *c* with a rate constant of 5×10^5 s^{-1} (*26*). Laser flash photolysis of a 1:1 complex between Ru-39-C*c* and wild-type C*c*O at low ionic strength led to intracomplex electron transfer from heme *c* to Cu_A in C*c*O with a rate constant k_a of 76000 ± 15000 s^{-1}, followed by electron transfer from Cu_A to heme *a* with rate constant k_b (Figure 8, Scheme 1).

The rate constant for reduction of heme *a* measured at 600 nm in this experiment is the same as the rate constant for oxidation of heme *c* measured at 550 nm, indicating that k_a is rate-limiting and k_b is faster than k_a. k_b was measured to be 90000 s^{-1} using a ruthenium dimer which directly reduces Cu_A within 1 μs (*32*). Increasing the ionic strength did not affect the rate constant k_a, but above 50 mM the amplitude of the fast intracomplex phase decreased, indicating complex dissociation, and a new slower phase appeared due to bimolecular reaction of uncomplexed Ru-39-C*c* with C*c*O (Figure 8, Scheme 1). The ratio between the absorbance changes associated with the fast intracomplex phase and the slow bimolecular phase was used to determine the equilibrium dissociation constant K_d of the Ru-39-C*c*:C*c*O complex to be 20 ± 6 μM at 55 mM ionic strength. The pseudo-first-order rate constant k_{obs} of the slow bimolecular phase reached a maximum at 75 mM ionic strength and deceased with further increases in ionic strength.

The reaction of Ru-39-C*c* with S44G C*c*O was nearly the same as that with wild-type C*c*O (Figure 8). The rate constant

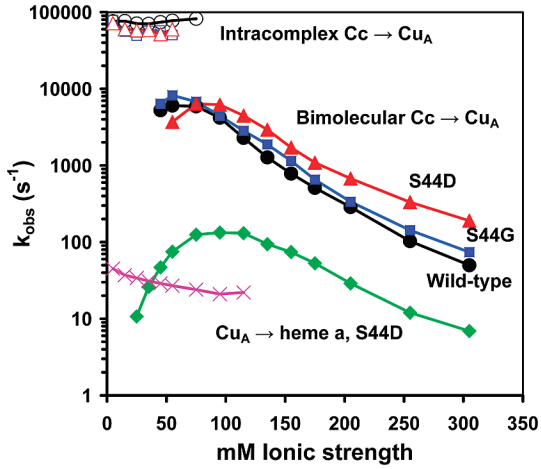

FIGURE 8: Ionic strength dependence of reaction of Ru-39-C*c* with native C*c*O, S44G C*c*O, and S44D C*c*O at pH 8.0. The solutions contained 12 μM Ru-39-C*c*, 15 μM C*c*O, 5 mM Tris-HCl, pH 8.0, 10 mM aniline, 1 mM 3CP, 0−300 mM NaCl, and 0.1% lauryl maltoside. Wild-type C*c*O: ○ (black), intracomplex k_a; ● (black), bimolecular k_{aobs}. S44G C*c*O: □ (blue), intracomplex k_a; ■ (blue), bimolecular k_{aobs}. S44D C*c*O: △ (red), intracomplex k_a; ▲ (red), bimolecular k_{aobs}; ◆ (green), k_b. Reaction of 20 μM Ru_2Z with 13 μM S44D C*c*O, × (magenta).

k_a for intracomplex electron transfer from Ru-39-C*c* to S44G was 79000 ± 15000 s^{-1} at low ionic strength, the equilibrium dissociation constant K_d was 18 ± 7 at 55 mM ionic strength, and the ionic strength dependence of the bimolecular phase was similar to that of wild type. The ratio of heme *a* to Cu_A reduced after equilibrium has been reached was 4.3 for S44G C*c*O, which indicates that the redox potential of heme *a* is 37 mV higher than Cu_A. This ratio was 6.1 for wild-type C*c*O, indicating a redox potential difference of 46 mV, suggesting an ~10 mV lowering of the heme *a* redox potential in the S44G mutant.

The initial reaction of Ru-39-C*c* with Cu_A in S44D C*c*O was also similar to that of wild-type C*c*O at pH 8.0 (Figure 8). The rate constant k_a for intracomplex electron transfer from photoreduced heme *c* to Cu_A was 71000 ± 15000 s^{-1} at low ionic strength. The equilibrium dissociation constant K_d was 12 ± 4 at 55 mM ionic strength, and the ionic strength dependence of the bimolecular phase was similar to that of wild type, indicating that this mutant did not greatly affect the interaction of Ru-39-C*c* with the oxidase. However, electron transfer from Cu_A to heme *a* was dramatically different from wild type. At pH 8.0 and 75 mM ionic strength, Cu_A, monitored at 830 nm, was reduced with a rate constant of 6400 s^{-1} and then reoxidized with a rate constant of 125 s^{-1} (Figure 9). Heme *a*, monitored at 600 nm, was reduced with a rate constant of 125 s^{-1} (Figure 9). Therefore, the rate constant k_b for electron transfer from Cu_A to heme *a* is 125 s^{-1} for S44D C*c*O, compared to 90000 s^{-1} for wild-type C*c*O. The 830 nm transient recovered to the preflash baseline after equilibrium was reached (Figure 9), indicating that Cu_A was completely reoxidized. The ratio of heme *a* to Cu_A reduced after equilibrium was reached was >10 for S44D C*c*O.

Unexpectedly, the intramolecular rate constant k_b for heme *a* reduction in S44D was found to be affected by both C*c* binding and ionic strength in a complex fashion (Figures 8 and 10). The rate constant k_b is very slow, 10 s^{-1}, at 25 mM ionic strength where S44D C*c*O and Ru-39-C*c* are in a tight

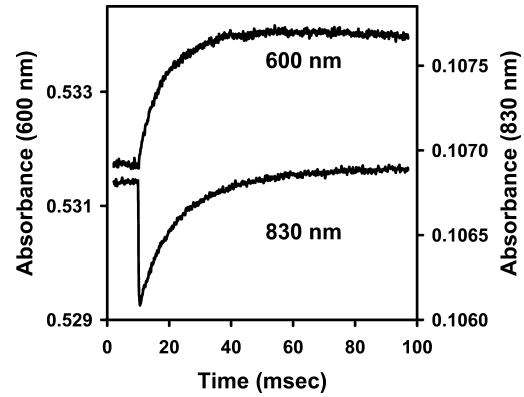

FIGURE 9: Photoinduced electron transfer from 12 μM Ru-39-C*c* to 15 μM S44D C*c*O under the same conditions as in Figure 8 with 70 mM NaCl. Absorbance transients are shown at 830 and 600 nm.

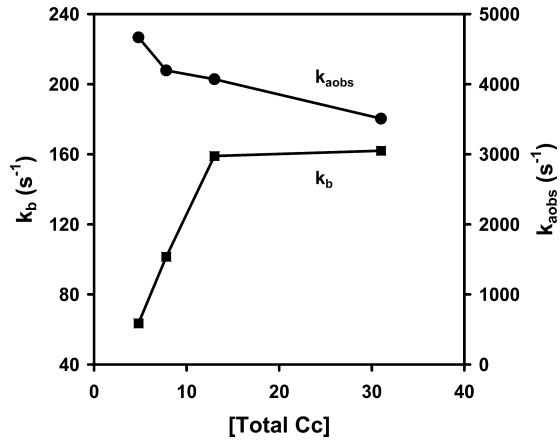

FIGURE 10: Effect of native horse C*c* on the reaction of 4.8 μM Ru-39-C*c* with 5.8 μM S44D CcO under the same conditions as in Figure 8 with 70 mM NaCl. The total C*c* concentration shown is the sum of the Ru-39-C*c* and native C*c* concentrations.

1:1 complex (Figure 8). k_b increases to a maximum of 125 s^{-1} as the ionic strength is increased to 75 mM at a constant Ru-39-C*c* concentration of 12 μM and then decreases with further increases in ionic strength (Figure 8). To explore the effect of C*c* binding on k_b, the reaction of 4.8 μM Ru-39-C*c* with 5.8 μM S44D C*c*O was studied at 75 mM ionic strength as a function of added native horse C*c* (Figure 10). Under these conditions Ru-39-C*c* is largely dissociated from C*c*O, and both Ru-39-C*c* and native horse C*c* are rapidly binding and dissociating from C*c*O. The rate constant k_b increased from 63 s^{-1} in the absence of unlabeled C*c* to 160 s^{-1} in the presence of excess C*c*. Taken together, the results of Figures 8 and 10 indicate that both ionic strength and cytochrome *c* binding have a significant effect on k_b. In the presence of saturating C*c* or Ru-39-C*c*, k_b increases from 10 to 160 s^{-1} as the ionic strength is increased from 25 to 75 mM.

The kinetics of electron transfer from Cu_A to heme *a* in S44D C*c*O was also examined by using the ruthenium dimer Ru_2Z to rapidly reduce Cu_A (Figure 8). The rate constant k_d decreased from 45 s^{-1} at 5 mM ionic strength to 22 s^{-1} at 110 mM ionic strength, showing only a small ionic strength effect (Figure 8) opposite to that observed when cytochrome *c* was present. The significance of this result is difficult to assess, however, since Ru_2Z also binds to the oxidase at low ionic strength and may have its own effect on the rate of heme *a* reduction.

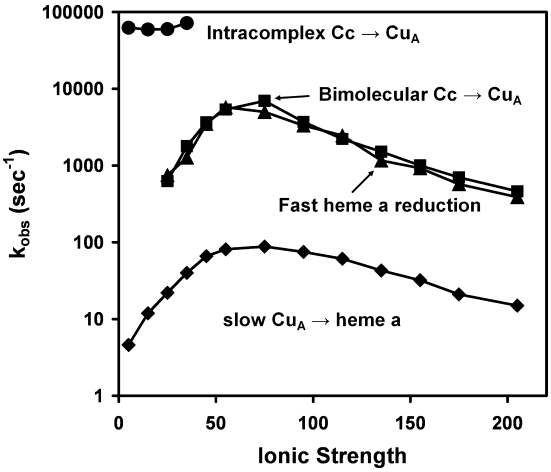

FIGURE 11: Ionic strength dependence of reaction of Ru-39-C*c* with S44D C*c*O in 5 mM sodium phosphate, pH 6.5, 10 mM aniline, 1 mM 3CP, 0−300 mM NaCl, and 0.1% lauryl maltoside, following the C*c* at 550 nm, Cu_A at 830 nm, and heme *a* at 600 nm. Key: ●, intracomplex k_a; ■, bimolecular k_{aobs} measured at 550 nm; ▲, fast phase of reduction of heme *a* measured at 600 nm; ◆, slow phase of reduction of heme *a*.

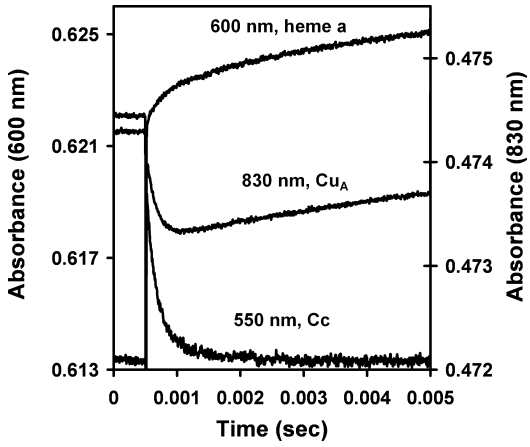

FIGURE 12: Time course of photoinduced electron transfer from Ru-39-C*c* S44D C*c*O at pH 6.5. The conditions are the same as in Figure 11 with 70 mM NaCl over a short time scale.

As the pH is decreased below pH 8.0, a new fast phase appears in the reduction of heme *a* in S44D C*c*O. The reaction between Ru-39-C*c* and Cu_A is very similar at pH 6.5 to that at pH 8.0, with an intracomplex rate constant k_a of 72000 ± 10000 s^{-1} at low ionic strength and a slower bimolecular phase at higher ionic strength (Figure 11). However, the reduction of heme *a* is biphasic, with a fast phase like wild type with the same rate constant as heme *c* oxidation and Cu_A reduction at all ionic strengths, indicating that the fast phase of electron transfer from Cu_A to heme *a* is faster than the rate-limiting reduction of Cu_A (k_b(intracomplex) > 30000 s^{-1}) (Figures 11 and 12). The rate constant of the slow phase of heme *a* reduction has similar ionic strength dependence at pH 6.5 as at pH 8.0, reaching a maximum of 90 s^{-1} at 70 mM ionic strength (Figure 11). The pH dependence of electron transfer from Cu_A to heme *a* was studied at a constant ionic strength of 75 mM (Figures 13 and 14). Percentage of the fast phase increased from 0% at pH 8.0 to 52% at pH 5.0, while the rate constant of the slow phase decreased from 120 s^{-1} at pH 7.8 to 85 s^{-1} at pH 5.5 (Figure 13). The rate constants for the wild-type and S44 mutant forms are summarized in Table 3.

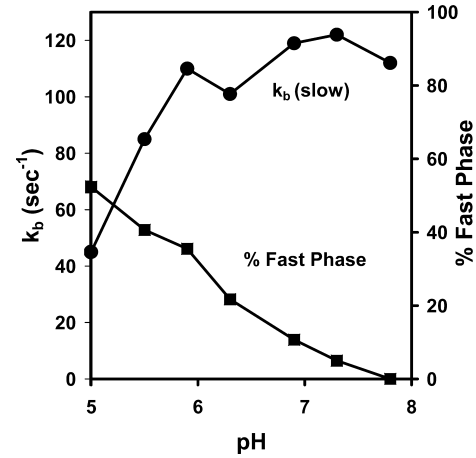

FIGURE 13: pH dependence of reaction of Ru-39-C*c* with S44D C*c*O in 10 mM aniline, 1 mM 3CP, 70 mM NaCl, 0.1% lauryl maltoside, and 5 mM buffer (a mixture of Tris-HCl, MES, and acetate). (●) The rate constant of the slow phase of reduction of heme *a*, k_b. (■) The % fast phase of reduction of heme *a*.

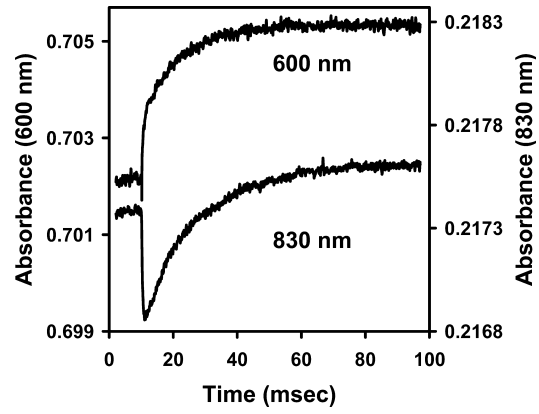

FIGURE 14: Time course of photoinduced electron transfer from Ru-39-C*c* S44D C*c*O at pH 5.5, following Cu_A at 830 nm and heme *a* at 600 nm. The conditions are the same as in Figure 13 with 70 mM NaCl.

Table 3: Summary of Fast Electron Transfer Characteristics for Cu_A to Heme *a* in Wild Type and S44 Mutants of C*c*O

C*c*O	K (k_b/k_c)	ΔE_m (mV) heme *a*−Cu_A	k_a ($\times 10^4$ s^{-1})	k_b (s^{-1}) fast phase	k_b (s^{-1}) slow phase	K_d[b]
wild type	6.1	46	7.6 ± 1.5	90000		20 ± 6
S44G	4.3	37	7.9 ± 1.5	>80000		18 ± 7
S44D, pH 8	>10	>60[a]	7.1 ± 1.5		10−125	12 ± 4
S44D, pH 6.5	>10	>60[a]	7.2 ± 1	>30000	5−90	

[a] See text for discussion of apparent change in redox potential with protonation state. [b] Measured at 55 mM ionic strength.

When the EPR spectra were measured at pH 5.5−8.0 a similar shift in the intensities of the two peaks at $g_z = 2.72$ (high pH) and $g_z = 2.78$ (low pH) was seen (Figure 7B), suggesting that both the EPR and the electron transfer rates were influenced by the same protonation event.

The deuterium solvent isotope effect was measured under the conditions of Figure 8 with 12.6 μM S44D C*c*O and 7.9 μM Ru-39-C*c* in 5 mM Tris-HCl, pH 8.0, with 90 mM NaCl. One sample contained 100% H_2O with a pH meter reading of 8.0, while the other sample contained 95% D_2O with a pH meter reading of 7.6, which is equivalent to a pD of 8.0

(*33*). The deuterium solvent isotope ratio $k_b(H_2O)/k_v(D_2O)$ was 1.2 ± 0.1 (data not shown).

DISCUSSION

Spectroscopic Measurements. In both mutant C*c*Os there are distinctive alterations in the paramagnetic spectra. The mutation of S44G shifts the heme *a* peak from $g_z = 2.82$ to $g_z = 2.86$, in the direction of the heme *a* EPR signal of bovine oxidase which has a peak at $g = 3.03$. Additionally, the S44G mutation causes a shift in the low-spin heme *a* g_x, from 1.63 to 1.60, and g_y, from 2.31 to 2.30. These changes are not reflected in the visible spectrum of the S44G which appears identical to wild type.

Despite the shift of the heme *a* g_z signal in S44G to a value closer to that of the bovine C*c*O, the shift by no means completely explains the major difference between the EPR spectra of *Rs* and bovine C*c*O. The remaining difference could be due to other residues that surround the histidine ligand on the same side as the glycine, which are not hydrogen-bonded to the histidine. These less conserved residues are mostly hydrophobic and aromatic and could affect the electronic configuration, augmenting the difference between the serine and the glycine hydrogen bonds (see EPR paper (*11*)).

It is interesting that the type of heme, whether *b* or *a*, has little influence on the g_z signal of the low-spin heme. The ba_3 oxidase from *T. thermophilus* (*17*) has an EPR signal for its low-spin heme *b* of $g_z = 3.08$, more like that of the bovine oxidase $g_z = 3.03$, than the low-spin heme *a* of *Rs* C*c*O. The similarities in the EPR signals of bovine and ba_3 oxidases are more related to the hydrogen-bonding partner of the histidine ligand, as both have a glycine backbone carbonyl.

The S44D mutation shifts the EPR peaks in the opposite direction to S44G, giving rise to a major split peak at $g_z =$ 2.72/2.78 (wild-type $g_z = 2.82$) and a split peak at $g_y = 1.74/$ 1.68 (wild-type $g_z = 1.63$). These results are suggestive of two different forms or conformations of the carboxylic acid that has replaced the usual hydroxyl in the case of S44. These major shifts in the EPR spectrum are accompanied by relatively minor changes in the visible spectrum. Initially, the visible spectrum looked unaltered as in the case of the S44G mutation, but more careful examination revealed that there was a somewhat variable lowering of the apparent extinction coefficient at 606 nm compared to 444 nm, by 20−30%. The variability was related to pH and ionic conditions, with the lowest extinction at higher pH. This is consistent with the likely different configurations of the carboxylate in its association with the heme and with the fact that the relative intensities of the EPR peaks are also strongly influenced by pH. The data from spectral and kinetic measurements support the hypothesis that S44D can exist in protonated and unprotonated forms and likely more than one conformation of each. The interaction of this anionic, protonatable residue with the histidine ligand (H102) of heme *a* appears to have considerable influence over the electronic configuration of the low-spin heme *a*, resulting in an altered EPR spectrum that is sensitive to bulk pH and altered kinetics of electron transfer.

Crystal structures of both the oxidized and reduced forms of the S44D mutant at 2.8 Å resolution show that the carboxyl is not well resolved in the oxidized form, but the reduced state clearly shows the carboxyl with one oxygen at 2.7 Å from the His 102 nitrogen. This is consistent with the results of kinetic analysis indicating that reduction leads to protonation of the carboxyl, restoring a native redox potential of heme *a*, and the EPR spectra indicating that protonation at low pH intensifies a g_z signal at 2.78.

Scheme 2

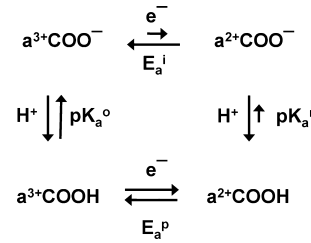

Effect of Mutation on Electron Transfer and Redox Potential. The mutation of S44 to glycine causes little change of redox potential in heme *a*. The small change, ∼10 mV, to a less positive redox potential relative to Cu_A, may be produced by subtle changes in the region around heme *a* such as a rearrangement of water. The change is not sufficient to cause any major alteration in the kinetic behavior, as shown in steady-state, stopped-flow, and photoinduced rapid kinetic measurements reported here. It is also not in the direction, nor of the magnitude, expected if the Ser to Gly mutation were to account for the main differences between the hemes *a* of bovine and *Rs* oxidases. The wild-type *Rs* C*c*O has a redox potential of heme *a* relative to Cu_A that is already ∼13 mV less positive than for the bovine C*c*O (*12*).

In the S44D mutant, in contrast, the kinetics of electron transfer from Cu_A to heme *a* are dramatically altered, with a distinctive pH dependence such that at high pH the rate is slowed compared to wild type by a factor of 1000, but as the pH is lowered, an increasing proportion of the rate reverts to wild type. These observations, along with pH-dependent EPR changes, are most easily rationalized as being due to the ionization state of the aspartate carboxyl group (Scheme 2). At pH 8.0 and 7.4, it is likely that D44 is mostly deprotonated, greatly decreasing the positive redox potential of heme *a* and inhibiting its rapid reduction. The very slow rate of electron transfer from Cu_A to heme *a* could then be accounted for by its dependence on the rate of proton uptake needed to convert the deprotonated D44 to its protonated form, stabilizing heme *a* reduction by raising its effective redox potential. This would be a true proton-coupled electron transfer mechanism. When heme *a* is oxidized, the positive charge on the heme is stabilized by the negative charge on the deprotonated D44, making reduction of heme *a* very unfavorable. The fact that the rate of electron transfer at high pH is slow but the reaction goes to completion indicates that eventually D44 is protonated and heme *a* assumes a high redox potential. The initial state would contain oxidized heme *a* with a low redox potential and ionized Asp 44 (a^{3+} COO^-), while the final state would contain reduced heme *a* with a high redox potential and protonated D44 (a^{2+} COOH). This provides a good example of linkage between the redox potential of heme *a* (E_a^i and E_a^p for the ionized and protonated states) and the pK_a of D (pK_a^o and pK_a^r) for the oxidized and reduced states. At pH 6.5, D44 has a mixture of protonated/deprotonated forms, consistent with the EPR

spectra, and this gives rise to the observed biphasic kinetics. The fraction that it is protonated will result in rapid electron transfer from Cu_A to heme *a*, as in wild-type C*c*O. The fraction with deprotonated D44 will result in a very slow rate of electron transfer from Cu_A to heme *a*, which is rate-limited by the protonation of D44.

There are at least four different reaction modes for the proton-coupled electron transfer mechanism shown in Scheme 2 (*34*). Electron transfer could either precede or follow proton transfer, and either proton transfer or electron transfer could be rate-limiting. Graige et al. (*34*) have developed expressions for the rate constant of the reaction for each of these different modes. Since both slow and fast phases of the reaction are observed at intermediate pH values between 5 and 6.5, the rate of proton transfer must be slower than the rate of electron transfer and, hence, rate-limiting. If rate-limiting proton transfer precedes electron transfer, then the slow phase of electron transfer will proceed along the lower pathway of Scheme 2:

$$a^{3+}\,\mathrm{COO}^- \overset{\mathrm{H^+}}{\rightleftharpoons} a^{3+}\,\mathrm{COOH} \overset{\mathrm{e^-}}{\rightleftharpoons} a^{2+}\,\mathrm{COOH}$$

The observed rate constant for electron transfer from Cu_A to heme *a* will be

$$k_b = k_H^{\,o} \tag{1}$$

where $k_H^{\,o}$ is the rate-limiting rate constant for proton transfer to D44 with heme *a* oxidized (*34*). In this case, the rate constant $k_H^{\,o}$ for proton transfer would be equal to the observed rate constant k_b, or about 125 s^{-1} at 75 mM ionic strength, pH 8.0. If on the other hand rate-limiting proton transfer follows initial rapid-equilibrium electron transfer, then the slow phase of electron transfer will proceed along the upper pathway of Scheme 2:

$$a^{3+}\,\mathrm{COO}^- \overset{\mathrm{e^-}}{\rightleftharpoons} a^{2+}\,\mathrm{COO}^- \overset{\mathrm{H^+}}{\rightleftharpoons} a^{2+}\,\mathrm{COOH}$$

In this case, the observed rate constant k_b would be

$$k_b = f(a^{2+}\,\mathrm{COO}^-)k_H \tag{2}$$

where $f(a^{2+}\,\mathrm{COO}^-)$ is the fraction of protein in the state ($a^{2+}\,\mathrm{COO}^-$) and $k_H^{\,r}$ is the rate constant for proton transfer to D44 with heme *a* reduced (*34*). Since no fast phase for k_b was observed at pH 8.0 within an experimental error of 5%, $f(a^{2+}\,\mathrm{COO}^-)$ is estimated to be less than 0.05. With this fraction of heme *a* reduced, the redox potential of heme *a* with D44 ionized, $E_a^{\,i}$, is estimated to more than 80 mV smaller than the redox potential of Cu_A, compared to wild-type C*c*O where the redox potential of heme *a* is 46 mV higher than that of Cu_A. $k_H^{\,r}$ is estimated to be greater than 2500 s^{-1} from eq 2 using $f(a^{2+}\,\mathrm{COO}^-) > 0.05$ and $k_b = 125$ s^{-1}. Unfortunately, it is not possible to determine from the present results whether rate-limiting proton transfer precedes or follows electron transfer. The rate constant k_b does not increase with decreasing pH (Figure 13), and moreover the deuterium solvent isotope effect for k_b is relatively small, 1.2 ± 0.1. Both of these observations indicate that proton transfer itself is not rate-limiting. However, a slow, rate-limiting, conformational change which controls proton transfer to D44 would be consistent with all of the results. It is remarkable that C*c* binding and ionic strength have such a large effect on the k_b and, hence, this postulated conformational change.

These results raise an interesting question: where do the protons come from to protonate D44? It is noteworthy that the S44D mutant is somewhat inefficient at proton pumping, suggesting the possibility that the proton required for heme *a* reduction (D44 protonation) does not come from outside the protein but is initially taken internally from the pumping path. This interpretation is consistent with the lack of a significant deuterium isotope effect, the lack of differential inhibition of the S44D mutant by zinc (Table 1), and the lack of stimulation by low bulk pH of the *rate* of the slow phase of electron transfer from Cu_A to heme *a* (Figure 13).

Given the described characteristics of the S44D mutant, it is of interest as a model for proton-coupled electron transfer and as a potential tool for studying the effect of slowed kinetics in the Cu_A to heme *a* step on the subsequent proton and electron transfer reactions in cytochrome *c* oxidase.

ACKNOWLEDGMENT

We thank Dr. D. Proshylakov for providing the CO for spectra, Dr. Rajendra Bose Muthukumaran for making the initial EPR spectral analysis of the S44G mutant form, and Dr. J. Hosler for helpful suggestions on the visible spectral analysis.

REFERENCES

1. Hosler, J. P., Ferguson-Miller, S., and Mills, D. A. (2006) Energy Transduction: Proton Transfer Through the Respiratory Complexes, in *Annual Reviews in Biochemistry* (Kornberg, R. P., Raetz, C. R. H., Rothman, J. E., and Throner, J. W., Eds.) Vol. 75, pp 165−187, Palo Alto, CA (Annual Reviews).
2. Belevich, I., Bloch, D. A., Belevich, N., Wikstrom, M., and Verkhovsky, M. I. (2007) Exploring the proton pump mechanism of cytochrome *c* oxidase in real time. *Proc. Natl. Acad. Sci. U.S.A. 104*, 2685–2690.
3. Jasaitis, A., Rappaport, F., Pilet, E., Liebl, U., and Vos, M. H. (2005) Activationless electron transfer through the hydrophobic core of cytochrome *c* oxidase. *Proc. Natl. Acad. Sci. U.S.A. 102*, 10882–10886.
4. Rich, P., Meunier, B., Mitchell, R., and Moody, R. (1996) Coupling of charge and proton movement in cytochrome *c* oxidase. *Biochim. Biophys. Acta 1275*, 91–95.
5. Wikstrom, M. (1988) How does cytochrome oxidase pump protons? A "cooperative proton pump" model. *Ann. N.Y. Acad. Sci. 550*, 199–206.
6. Brzezinski, P., and Larsson, G. (2003) Redox-driven proton pumping by heme-copper oxidases. *Biochim. Biophys. Acta 1605*, 1–13.
7. Wikstrom, M. (1988) Protonic sidedness of the binuclear iron-copper centre in cytochrome oxidase. *FEBS Lett. 231*, 247–252.
8. Tsukihara, T., Aoyama, H., Yamashita, E., Tomizaki, T., Yamaguchi, H., Shinzawa-Itoh, K., Nakashima, R., Yaono, R., and Yoshikawa, S. (1995) Structures of metal sites of oxidized bovine heart cytochrome *c* oxidase at 2.8Å. *Proc. Natl. Acad. Sci. U.S.A. Science 269*, 1069–1074.
9. Iwata, S., Ostermeier, C., Ludwig, B., and Michel, H. (1995) Structure at 2.8. Å resolution of cytochrome *c* oxidase from *Paracoccus denitrificans*. *Nature 376*, 660–669.
10. Qin, L., Hiser, C., Mulichak, A., Garavito, R. M., and Ferguson-Miller, S. (2006) Identification of conserved lipid/detergent-binding sites in a high-resolution structure of the membrane protein cytochrome *c* oxidase. *Proc. Natl. Acad. Sci. U.S.A. 103*, 16117–16122.
11. Hosler, J. P., Fetter, J., Tecklenburg, M. M. J., Espe, M., Lerma, C., and Ferguson-Miller, S. (1992) Cytochrome aa_3 of *Rhodobacter sphaeroides* as a model for mitochondrial cytochrome *c* oxidase. *J. Biol. Chem. 267*, 24264–24272.

12. Wang, K., Zhen, Y., Sadoski, R., Grinnell, S., Geren, L., Ferguson-Miller, S., Durham, B., and Millett, F. (1999) Definition of interaction domain for the reaction of cytochrome *c* with cytochrome *c* oxidase: II. Rapid kinetics analysis of electron transfer from cytochrome *c* to *Rhodobacter sphaeroides* cytochrome oxidase surface mutants. *J. Biol. Chem. 274*, 38042–38050.
13. Lee, H.-M., Das, T., Rousseau, D., Mills, D., Ferguson-Miller, S., and Gennis, R. (2000) Mutations in the putative H-channel in the cytochrome *c* oxidase from *Rhodobacter sphaeroides* show that this channel is not important for proton conduction but reveals modulation of the properties of heme *a*. *Biochemistry 39*, 2989–2996.
14. de Paula, J. C., Peiffer, W. E., Ingle, R. T., Centeno, J. A., Ferguson-Miller, S., and Babcock, G. T. (1990) Hemes *a* and a_3 environments of plant cytochrome *c* oxidase. *Biochemistry 29*, 8702–8706.
15. Mitchell, D. M., Adelroth, P., Hosler, J. P., Fetter, J. R., Brzezinski, P., Pressler, M. A., Aasa, R., Malmstrom, B. G., Alben, J. O., Babcock, G. T., Gennis, R. B., and Ferguson-Miller, S. (1996) A ligand-exchange mechanism of proton pumping involving tyrosine-422 of subunit I of cytochrome oxidase is ruled out. *Biochemistry 35*, 824–828.
16. Tsukihara, T., Aoyama, H., Yamashita, E., Tomizaki, T., Yamaguchi, H., Shinzawa-Itoh, K., Nakashima, R., Yaono, R., and Yoshikawa, S. (1996) The whole structure of the 13-subunit oxidized cytochrome *c* oxidase at 2.8 Å. *Science 272*, 1136–1144.
17. Zimmermann, B. H., Nitsche, C. I., Fee, J. A., Rusnak, F., and Mack, E. (1988) Properties of a copper-containing cytochrome ba_3: A second terminal oxidase from the extreme thermophile *Thermus Thermophilus*. *Proc. Natl. Acad. Sci. U.S.A. 85*, 5779–5783.
18. Horton, R. M., Hunt, H. D., Ho, S. N., Pullen, J. K., and Pease, L. R. (1989) Engineering hybrid genes without the use of restriction enzymes: Gene splicing by overlap extension. *Gene 77*, 61–68.
19. Mitchell, D. M., and Gennis, R. B. (1995) Rapid purification of wildtype and mutant cytochrome *c* oxidase from *Rhodobacter sphaeroides* by Ni^{2+}-NTA affinity chromatography. *FEBS Lett. 368*, 148–150.
20. Keen, N. T., Tamaki, S., Kobayashi, D., and Trollinger, D. (1988) Improved broad-host-range plasmids for DNA cloning in Gram-negative bacteria. *Gene 70*, 191–197.
21. Zhen, Y., Qian, J., Follmann, K., Hosler, J., Hayward, T., Nilsson, T., and Ferguson-Miller, S. (1998) Overexpression and purification of cytochrome *c* oxidase from *Rhodobacter sphaeroides*. *Protein Expression Purif. 13*, 326–336.
22. Simon, R., Priefer, U., and Puhler, A. (1983) A broad host range mobilization system for *in vivo* genetic engineering: Transposon mutagenesis in Gram negative bacteria. *Bio/Technology 1*, 784–791.
23. Shapleigh, J. P., and Gennis, R. B. (1992) Cloning, sequencing, and deletion from the chromosome of the gene encoding subunit I of the aa^3-type cytochrome *c* oxidase of *Rhodobacter sphaeroides*. *Mol. Microbiol. 6*, 635–642.
24. Hiser, C., Mills, D. A., Schall, M., and Ferguson-Miller, S. (2001) C-terminal truncation and histidine-tagging of cytochrome *c* oxidase subunit II reveals the native processing site, shows involvement of the C-terminus in cytochrome *c* binding, and improves the assay for proton pumping. *Biochemistry 40*, 1606–1615.
25. Mills, D. A., Schmidt, B., Hiser, C., Westley, E., and Ferguson-Miller, S. (2002) Membrane potential-controlled inhibition of cytochrome *c* oxidase. *J. Biol. Chem. 277*, 14894–14901.
26. Geren, L. M., Beasley, J. R., Fine, B. R., Saunders, A. J., Hibdon, S., Pielak, G. J., Durham, B., and Millett, F. (1995) Design of a ruthenium-cytochrome *c* derivative to measure electron transfer to the initial acceptor in cytochrome *c* oxidase. *J. Biol. Chem. 270*, 2466–2662.
27. Patel, C. N., Lind, M. C., and Pielak, G. J. (2001) Characterization of horse cytochrome *c* expressed in *Escherichia coli*. *Protein Expression Purif. 22*, 220–224.
28. Engstrom, G., Rajagukguk, R., Saunders, A. J., Patel, C. N., Rajagukguk, S., Merbitz-Zahradnik, T., Xiao, K., Pielak, G. J., Trumpower, B., Yu, C.-A., Yu, L., Durham, B., and Millett, F. (2003) Design of a ruthenium-labeled cytochrome *c* derivative to study electron transfer with the cytochrome bc_1 complex. *Biochemistry 42*, 2816–2824.
29. Liu, R. Q., Geren, L., erson, P., Fairris, J. L., Peffer, N., McKee, A., Durham, B., and Millett, F. (1995) Design of ruthenium-cytochrome *c* derivatives to measure electron transfer to cytochrome *c* peroxidase. *Biochimie 77*, 549–561.
30. Brand, S. E., Rajagukguk, S., Ganesan, K., Geren, L., Fabian, M., Han, D., Gennis, R. B., Durham, B., and Millett, F. (2007) A new ruthenium complex to study single-electron reduction of the pulsed OH state of detergent-solubilized cytochrome oxidase. *Biochemistry 46*, 14610–14618.
31. Mills, D. A., Geren, L., Hiser, C., Schmidt, B., Durham, B., Millett, F., and Ferguson-Miller, S. (2005) An arginine to lysine mutation in the vicinity of the heme propionates affects the redox potentials of the hemes and associated electron and proton transfer in cytochrome *c* oxidase. *Biochemistry 44*, 10457–10465.
32. Zaslavsky, D., Sadoski, R. C., Wang, K., Durham, B., Gennis, R. B., and Millett, F. (1998) Single electron reduction of cytochrome *c* oxidase compound F: resolution of partial steps by transient spectroscopy. *Biochemistry 37*, 14910–14916.
33. Schowen, K. B., and Schowen, R. L. (1982) Solvent isotope effects of enzyme systems. *Methods Enzymol. 87*, 551–606.
34. Graige, M. S., Paddock, M. L., Bruce, J. M., Feher, G., and Okamura, M. Y. (1996) Mechanism of proton-coupled electron transfer for quinone (QB) reduction in reaction centers of *Rhodopseudomonas sphaeroides*. *J. Am. Chem. Soc. 118*, 9005–9016.

BI801156S